

## Post-collisional Stark mixing in Auger processes

J. E. Miraglia\* and J. Macek

University of Tennessee, Knoxville, Tennessee 37996  
and Oak Ridge National Laboratory, Oak Ridge, Tennessee 37831

(Received 9 May 1990)

Post-collisional effects on the electronic distribution of autoionization processes are studied. A formulation including both the long range of the projectile Coulomb potential and the polarization potential is presented. The latter potential mixes close lying levels of autoionizing states with equal magnetic quantum number, giving rise to a significant perturbation of the angular and energy distribution of the electron spectra. Particular attention is paid to the mixing of autoionizing levels of helium  $2s2p^1P$  and  $2p^2^1D$ . Deviation from  $90^\circ$  symmetry is studied, and comparison with experiments is presented.

### I. INTRODUCTION

When a multiple-electron target is excited by impact of a charged projectile, it may later decay, emitting one electron of a defined energy.<sup>1,2</sup> The electronic line shape corresponding to this autoionization or Auger process is affected by the outgoing projectile via the long-range potentials.<sup>3</sup> Three effects will be here mentioned that are relevant to the present work. First, the peak is shifted due to the Coulomb force of the projectile upon the target electrons; here this will be called the *binding* effect (see, for example, Devdariani, Ostroskii, and Sebayakin<sup>4</sup>). Second, a sharp enhancement of the profile in the forward direction is observed,<sup>5</sup> which is due to the post-collision Coulomb interaction between the ejected electron and the projectile; this effect is called *focusing*, and the theory was recently derived.<sup>6</sup> Third, the projectile-target interaction mixes close lying states and the angular distribution of the autoionization electrons deviates from symmetry about  $90^\circ$ ; this effect is called *Stark* mixing and was first observed by Stolterfoth, Brand and Prost.<sup>7</sup> The aim of the present work is to develop a general theory to treat the autoionization process involving the three mentioned effects, paying particular attention to the latter one.

Consider a point projectile of charge  $Z_p$  impinging with velocity  $v$  on a two (or more)-electron atom. Three time regions are relevant.

*Region I.*  $-t_0 < t < +t_0$ , the *internal* collision region where the excitation takes place via strong interaction with the projectile. For a typical collision, one has  $t_0 \sim r_0/v$ , where  $r_0$  is of the order of the size of the atom in the initial state. In this range, collisional amplitudes vary rapidly with time and impact parameter.

*Region II.*  $t_0 < t < t_1$ , the *external* or *post-collision* region where the energies of the states are shifted via the monopole part ( $1/vt$ ) of the projectile Coulomb potential and the states are mixed via the dipole term ( $\hat{v} \cdot \mathbf{r}/v^2 t^2$ ). The collisional amplitudes here vary only with time, and the impact parameter can be neglected. The coupling with the continuum can be also neglected, provided that  $t_1 \ll 2/\Gamma_L$ , where  $\Gamma_L^{-1}$  is the mean life of the excited

state. This work is designed to describe better this range and to investigate its influence in the electron spectra.

*Region III.*  $t_1 < t \sim 2/\Gamma_L$ , the *decaying* region. In this range, the collision has effectively ended and the states decay exponentially.

By inspecting the energy distribution of the Auger electrons, one is able to "map" the behavior of the transition amplitude as a function of time. Roughly speaking, electron energies ( $E$ ) near the unperturbed peak energy ( $E_L$ ) correspond to amplitudes at  $t \sim \Gamma_L^{-1}$  (region III). Energies at the tails of the peak correspond to shorter times, thus mapping amplitudes within region II (effects of the Stark mixing, if observable, should be found here). In the extreme wings of the distribution we would be transforming amplitudes within region I.

Although a general formalism is proposed in Sec. II, we will be concentrated mainly in the process:  $Z_p + \text{He} \rightarrow Z_p + \text{He}^{**}$ , the latter decaying to  $\text{He}^+(1s) + e$ . Several experiments were made with  $\text{He}^+$  as projectile,<sup>8,9</sup> and the spectra show structures due to Auger lines of both the target and the projectile.<sup>10</sup> In this work, we will consider the projectile as a point particle (nonemitter). Its consideration as emitter is straightforward [see Eq. (2.31)]. Atomic units are used except where indicated.

In the present work, we are interested in three autoionizing levels of the He atom:  $2s^2^1S$ ,  $2s2p^1P$ , and  $2p^2^1D$ . The corresponding states will be denoted only with the quantum numbers  $LM$  with  $M$  ranging from  $-L$  to  $L$ . Resonant or unperturbed peak energies ( $E_{LM} = E_L$ ) and full widths ( $\Gamma_{LM} = \Gamma_L$ ) are,  $E_0 = 1.222$ ,  $E_1 = 1.307$ ,  $E_2 = 1.298$ ; and  $\Gamma_0 = 0.005$ ,  $\Gamma_1 = 0.00153$ , and  $\Gamma_2 = 0.00263$ . Now, we introduce a reference time  $\Delta_{12}^{-1}$ , where  $\Delta_{12} = E_1 - E_2$  is the difference in energy levels. For the states  $2s2p^1P$  and  $2p^2^1D$ ,  $\Delta_{12}^{-1} = 110$  a.u., which falls well within region II. Differences involving the  $1S$  level correspond to even shorter times.

### II. THEORY

The final amplitude  $b_f(\rho, t)$  representing one electron in the ground state and the other in the continuum is given by<sup>1</sup>

$$i \frac{\partial}{\partial t} b_j(\rho, t) = \sum_j \exp[i(E - E_j)t] \langle \Psi_f^- | 1/r_{12} | \Phi_j \rangle \times b_j(\rho, t), \quad (2.1)$$

where  $E = k^2/2$  is the kinetic energy of the ejected electron,  $E_j = \epsilon_j - E_f$  is the resonant or unperturbed peak energy,  $\epsilon_j$  is the initial energy of the two-bound electrons, and  $E_f$  is the final ground-state energy [ $E_f = -2$  in the case of  $\text{He}^+(1s)$ ]. Also in Eq. (2.1)  $\rho$  is the impact parameter,  $t$  is the time,  $\Phi_j(\mathbf{r}_{T1}, \mathbf{r}_{T2})$  is the double-excited state,  $1/r_{12}$  is the usual electronic repulsion, and  $\Psi_f^-$  is the distorted final state. The amplitudes of the autoionizing states  $b_j(\rho, t)$  are themselves coupled and to the continuum states by the following relation:<sup>1</sup>

$$i \frac{\partial}{\partial t} b_j(\rho, t) = \sum_k \exp[i(E_j - E_k)t] \langle \Phi_j | V_P | \Phi_k \rangle b_k(\rho, t) + \int d\mathbf{k} \exp[i(E_j - E)t] \times \langle \Phi_j | 1/r_{12} | \Phi_f \rangle b_f(\rho, t), \quad (2.2)$$

where  $V_P = V_{P1} + V_{P2}$ ,  $V_{P1,2} = -Z_P/r_{P1,2}$  are the projectile electron Coulomb potentials. The coordinates  $\mathbf{r}_{T1,2}$  denote the positions of the electrons 1 and 2 with respect to the target and  $\mathbf{r}_{P1,2} = \mathbf{r}_{T1,2} - \mathbf{R}$  are the positions with respect to the projectile,  $\mathbf{R}$  being the internuclear distance.

In the distorted-wave formalism we incorporate the Coulomb interaction in the final channel, as follows:

$$\Psi_f^- = \Phi_f(\mathbf{r}_{T1}, \mathbf{r}_{T2}) D^-(a, -\mathbf{v}, \mathbf{r}_{P2}) D^-(a', \mathbf{v}', \mathbf{r}_{P1}), \quad (2.3)$$

where  $a = Z_P/v$ ,  $a' = Z_P/v'$ ,  $\mathbf{v}' = \mathbf{k} - \mathbf{v}$ , and

$$D^-(Z/p, \mathbf{p}, \mathbf{r}) = (1 + iZ/p) \exp[\pi(Z/p)/2] \times {}_1F_1(-iZ/p, 1, -ipr - i\mathbf{p} \cdot \mathbf{r}). \quad (2.4)$$

$\Phi_f(\mathbf{r}_{T1}, \mathbf{r}_{T2})$  is the unperturbed final state representing both electrons in the field of the target, one in the bound state and the other in the continuum. Since the initial state  $\Phi_j(\mathbf{r}_{T1}, \mathbf{r}_{T2})$  is peaked around  $r_{T1,2} \sim 0$  we can approximate  $\mathbf{r}_{P1,2} = \mathbf{r}_{T1,2} - \mathbf{R} \sim -\mathbf{R} \sim -\mathbf{v}t$ , and so

$$\langle \Psi_f^- | 1/r_{12} | \Phi_j \rangle \sim \langle \Phi_f | 1/r_{12} | \Phi_j \rangle D^{-*}(a, -\mathbf{v}, -\mathbf{v}t) \times D^{-*}(a', \mathbf{v}', -\mathbf{v}t), \quad (2.5)$$

where

$$D^{-*}(a, -\mathbf{v}, -\mathbf{v}t) = \Gamma(1 - ia) \exp(\pi a/2) \times {}_1F_1(ia, 1, iAt), \quad (2.6)$$

$$D^{-*}(a', \mathbf{v}', -\mathbf{v}t) = \Gamma(1 - ia') \exp(\pi a'/2) \times {}_1F_1(ia', 1, iA't),$$

and

$$A = 2v^2, \quad A' = (vv' - \mathbf{v} \cdot \mathbf{v}'). \quad (2.7)$$

The time limits of the Coulomb distortions factors are

$$D^{-*}(a, -\mathbf{v}, -\mathbf{v}t) \sim (At)^{-ia} \quad \text{for } t \gg 1/A, \quad (2.8)$$

$$D^{-*}(a', \mathbf{v}', -\mathbf{v}t) \rightarrow \begin{cases} \Gamma(1 - ia' \exp(\pi a'/2)) \\ (A't)^{-ia'} \end{cases} \begin{cases} \text{for } t \ll 1/A', \\ \text{for } t \gg 1/A'. \end{cases} \quad (2.9)$$

Equation (2.8) is a valid approximation in our case, but the equivalent expression in Eq. (2.9) is not always general (for example, in the forward direction  $A' = 0$ ).

Using Eq. (2.8) and factorizing out the long-distance Coulomb behavior of the doubly excited state<sup>11</sup> [see Eq. (3.2) below]:

$$b_j(\rho, t) = t^{2ia} C_j(\rho, t), \quad (2.10)$$

we have

$$ib_f(\rho) = \sum_j y_j \int_0^\infty \exp[i(E - E_j)t] t^{ia} \times D^{-*}(a', \mathbf{v}', -\mathbf{v}t) C_j(\rho, t), \quad (2.11)$$

where

$$y_j = \langle \Phi_f | 1/r_{12} | \Phi_j \rangle, \quad (2.12)$$

and the constant  $A^{-ia}$  was dropped. The inclusion of region I, i.e., the extension of the integral to  $t = 0$ , introduces no problem since the infinite oscillations of  $t^{ia}$  cancel any contribution coming from the internal collision range, region I. The remaining task then is to calculate  $C_j(\rho, t)$ .

#### A. No mixing of states

As a first approximation we neglect the interaction with the other excited states, and include only the coupling with the continuum to obtain the standard result

$$C_j(\rho, t) \sim C_j^{(0)}(\rho, t) = \exp(-\Gamma_j t/2) c_j(\rho, \infty), \quad (2.13)$$

where  $c_j(\rho, t = \infty)$  represents the collision amplitudes calculated at very long time. Substituting  $C_j^{(0)}$  into Eq. (2.11) gives the closed-form result

$$ib_f(\rho) = \sum_j F_j B_j \left[ \frac{y_j}{\omega_j} c_j(\rho, \infty) \right], \quad (2.14)$$

where

$$\omega_j = \frac{\Gamma_j}{2} + i(E_j - E), \quad (2.15)$$

$$B_j = \frac{\Gamma(1 + ia)}{\omega_j^{ia}}, \quad (2.16)$$

and

$$F_j = \Gamma(1 - ia') \exp(\pi a'/2) {}_2F_1(ia', 1 + ia, 1, iA'/\omega_j). \quad (2.17)$$

The three factors in Eq. (2.14) have precise physical meanings: the term in square brackets gives the Lorentz line shape in the absence of any projectile distortion,<sup>1</sup>  $F_j$  represents the focusing factor<sup>6</sup> which accounts for the

enhancement in the forward direction due to the interaction of the projectile with the ejected electron, and  $B_j$  is the binding correction<sup>4</sup> due to the long-distance Coulomb interaction with the bound electrons in the target and accounts for a shift of the peak energy. It will be found that Stark mixing introduces a fourth multiplicative factor in Eq. (2.14).

The factor  $F_j$  has the following limits:

$$F_j \rightarrow \begin{cases} \Gamma(1-ia')\exp(\pi a'/2) \text{ as } |A'/\omega_j| \ll 1, \\ \frac{\Gamma(1+i(a-a'))}{\Gamma(1+ia)} \left(\frac{A'}{\omega_j}\right)^{-ia'} \text{ as } |A'/\omega_j| \gg 1. \end{cases} \quad (2.18)$$

When  $a = a'$ , we have

$$F_j B_j(a = a') = \exp(-ia' \ln A') = \text{const}. \quad (2.19)$$

We call attention to a particular condition where focusing and binding effects cancel each other and shorter-range interactions, such as Stark mixing, should emerge more clearly. Since this happens at relatively high velocities, the shorter-range interactions are also weak and so the profile is expected to be unperturbed.

Integrating over the impact parameter gives the double differential cross section

$$\frac{d\sigma}{d\mathbf{k}} = \sum_{j,k} (y_j P_j)^* D_{j,k} (y_k P_k), \quad (2.20)$$

where

$$P_j = F_j B_j \frac{1}{\omega_j}, \quad (2.21)$$

and

$$D_{j,k} = \int d\rho c_j^*(\rho, \infty) c_k(\rho, \infty) \quad (2.22)$$

is the density-matrix element, the diagonal elements having the meaning of cross sections. In matrix form, we can write Eq. (2.20) as

$$\frac{d\sigma}{d\mathbf{k}} = (\mathbf{y} \cdot \mathbf{P})^* \mathbf{D} (\mathbf{y} \cdot \mathbf{P}) = (\mathbf{P}' \cdot \mathbf{y}')^\dagger \mathbf{D} (\mathbf{P}' \cdot \mathbf{y}'), \quad (2.23)$$

where  $y_j$  are components of a row vector  $\mathbf{y}$  ( $y'$ , the transposed, is a column vector),  $\mathbf{D}$  is the usual density matrix, and  $\mathbf{P}$  is a diagonal matrix, here called *profile* matrix. In general, as we shall see, the  $P$  matrix is nondiagonal owing to Stark mixing.

The factors  $y_j$  are, except for a constant, spherical harmonics [see Eq. (4.17) below] and account for the unperturbed electron angular distribution. The matrix elements  $P_j$  determine the profile of the electron energy distribution. They do not depend strongly upon the electron emission angle  $\theta$ , except in the forward direction where they take into account focusing effects<sup>6</sup> through  $F_j$ .  $D_{j,k}$  is a number which gives the intensity of the yield.

The two limits of Eq. (2.18) correspond to the asymptotic behaviors of  $D^{-*}(a', v', -vt)$ , in Eq. (2.9). In these

cases, the exponent of  $t$  (0 or  $-ia'$ ) adds to  $ia$  [see integrand of Eq. (2.11)] to produce a *total* Coulomb parameter  $\alpha$ , given by

$$\alpha = \begin{cases} a = \frac{Z_P}{v}, \text{ for } |A'/\omega_{LM}| \ll 1 \text{ (small angles)}, \\ a - a' = \frac{Z_P}{v} - \frac{Z_P}{v}, \text{ for } |A'/\omega_{LM}| \gg 1 \\ \text{(large angles)}. \end{cases} \quad (2.24)$$

At few-keV impact energies,  $a \gg a'$  and so  $\alpha = a$  with a good accuracy, but one should have in mind that as  $v$  increases  $\alpha$  decreases to the point that it vanishes [see Eq. (2.19)]. An exact expression of  $\alpha$  valid for all angles is not possible, since it is defined only through the limits, however, approximate expressions could be derived. For practical purposes, we use here the simple expression

$$\alpha = a - a' \frac{|A'|^2}{|A'|^2 + |\omega_{LM}|^2}, \quad (2.25)$$

which has the same limits of Eq. (2.24). By introducing the parameter  $\alpha$ , we will be able to estimate the effect of the Coulomb potential on the electron profile, as explained in Sec. IV.

Due to the long-distance monopole interaction, the maximum of the distribution  $E'_j$  is shifted with respect to the resonant position  $E_j$  by

$$E'_j - E_j = -\alpha \frac{\Gamma_j}{2}, \quad (2.26)$$

where the full width at half maximum (FWHM)  $\Gamma'_j$  is given by

$$\Gamma'_j \simeq \Gamma_j (1 + 1.15\alpha^2)^{1/2}. \quad (2.27)$$

When  $\alpha \gg 1$ ,  $\Gamma'_j \simeq \Gamma_j 0.81\alpha + \Gamma_j 0.26\alpha$ , where the first and second terms of the right-hand side correspond to the low-energy and high-energy half-widths of the peak, respectively. When focusing is neglected, or  $a \gg a'$ , then  $\alpha = a \gg 1$  and these Eqs. (2.26) and (2.27) become similar to Eq. (3) and (3') of Ref. 8. When  $a = a'$  or  $\alpha = 0$ ,  $E'_j = E_j$ , and  $\Gamma'_j = \Gamma_j$ , and the unperturbed distribution should be observed, as indicated before.

## B. Stark mixing

As an improved approximation we include the interaction with the other excited states, proposing

$$C_j(\rho, t) = \sum_k R_{j,k}(t) \exp[i(E_j - E_k)t] C_k^{(0)}(\rho, t), \quad (2.28)$$

where the terms  $R_{j,k}(t) \exp[i(E_j - E_k)t]$  represent solutions of the differential equation (2.2) in region II, with the condition that only channel  $k$  is populated at  $t \rightarrow \infty$ . In the present work we consider that the collision time is much smaller than the lifetime  $\Gamma_j$  and so we can neglect the coupling with the continuum included in the second term of the right-hand side of Eq. (2.2). The expression for the yields now reads

$$\frac{d\sigma}{d\mathbf{k}} = \sum_{j,k} \left[ \sum_n y_n P_{n,j} \right]^* D_{j,k} \left[ \sum_m y_m P_{m,k} \right], \quad (2.29)$$

where the matrix element  $P_{j,k}$  is given by

$$P_{j,k} = \int_0^\infty dt \exp(-\omega_k t) t^{ia} D^{-*}(a', \mathbf{v}', -\mathbf{v}t) R_{j,k}(t). \quad (2.30)$$

We recover Eq. (2.23) by decoupling the states, that is, assuming that  $R_{j,k}(t) = \delta_{j,k}$  so that  $P_{j,k} = P_j \delta_{j,k}$ . Note that we consider that  $R_{j,k}$  are only a function of time and not of impact parameter  $\rho$ , since we are interested in long collision time (region II) where the impact parameter can be neglected. Also note that  $R_{j,k}$  is a unitary matrix which relates the amplitudes at infinity to the amplitudes at time  $t$ .

If, as in many experimental situations, both the target (slower emitter) and the projectile (faster emitter) decay via Auger electrons and no coincident measurements are carried out, the total amplitudes then reads  $ib_f(\rho) = ib_f^{(T)}(\rho) + ib_f^{(P)}(\rho)$ , where the projectile quantities should include the Doppler effect. The double differential cross section is expressed in matrix form, as

$$\begin{aligned} \frac{d\sigma}{d\mathbf{k}} &= (\mathbf{y}^{(T)} \cdot \mathbf{P}^{(T)})^* \mathbf{D}^{(T,P)}(\mathbf{y}^{(T)} \cdot \mathbf{P}^{(T)})^t \\ &+ (\mathbf{y}^{(P)} \cdot \mathbf{P}^{(P)})^* \mathbf{D}^{(P,P)}(\mathbf{y}^{(P)} \cdot \mathbf{P}^{(P)})^t \\ &+ 2 \operatorname{Re}[(\mathbf{y}^{(T)} \cdot \mathbf{P}^{(T)})^* \mathbf{D}^{(T,P)}(\mathbf{y}^{(P)} \cdot \mathbf{P}^{(P)})^t], \end{aligned} \quad (2.31)$$

where the last term of the right-hand side involves a density matrix that mixes the amplitudes on the target and projectile. In this work we do not consider the projectile emission.

In Sec. III, we calculate the  $R$  matrix, and the  $P$ -matrix elements will be evaluated in Sec. IV. We summarize the findings in Sec. V, where the explicit expressions are written down.

### III. EVALUATION OF THE R-MATRIX ELEMENTS

In the close-coupling technique the wave function is proposed to be

$$\begin{aligned} \Phi_i(\mathbf{r}_{T_1}, \mathbf{r}_{T_2}, \rho, t) \\ = \sum_{L,M} b_{LM}(\rho, t) \exp(-i\varepsilon_{LM}t) \Phi_{LM}(\mathbf{r}_{T_1}, \mathbf{r}_{T_2}), \end{aligned} \quad (3.1)$$

where  $\Phi_{LM}$  is the standard combination of single electron wave functions  $\psi_{nlm}(\mathbf{r}_{T_{1,2}})$ . For the He-target case, the base is nine-dimensional ( $L$  from 0 to 2, and  $M$  from  $-L$  to  $L$ ), but we shall work in a six-dimensional base, by making use of the symmetry property:  $b_{L-M} = (-1)^M b_{LM}$ . Defining  $\Phi_{L\bar{M}} = [\Phi_{L-M} + (-1)^M \Phi_{LM}] / \sqrt{2}$  for  $M \neq 0$ , the corresponding amplitudes read  $b_{L\bar{M}} = (-1)^M \sqrt{2} b_{LM}$ ,  $\bar{M}$  ranging from 1 to  $L$ . Hereafter, the bar on  $M$  will be omitted. The amplitudes  $b_{LM}$  satisfy the differential equation given by Eq. (2.2), where we drop the second term of the right-hand side, because, as mentioned before, the backcoupling with the continuum can be neglected in this range (region II).

After some algebra, we find the diagonal matrix elements tend as

$$\langle \Phi_{LM} | V_P | \Phi_{LM} \rangle \rightarrow -\frac{2Z_P}{R} + O(1/R^3), \quad (3.2)$$

and this is the long-distance Coulomb behavior already incorporated in Eq. (2.10) above. The nondiagonal matrix elements of interest are the ones that have the same magnetic quantum number and the difference of orbital quantum numbers is unity. The asymptotic limits of these elements as  $R \rightarrow \infty$  are<sup>12</sup>

$$\langle \Phi_{00} | V_P | \Phi_{10} \rangle = \sqrt{2} \langle \psi_{200} | V_{P_1} | \psi_{210} \rangle \rightarrow -\frac{3\sqrt{2}Z_P}{Z_T R^2}, \quad (3.3)$$

$$\langle \Phi_{10} | V_P | \Phi_{20} \rangle = \frac{2}{\sqrt{3}} \langle \psi_{200} | V_{P_1} | \psi_{210} \rangle \rightarrow -\frac{2\sqrt{3}Z_P}{Z_T R^2}, \quad (3.4)$$

$$\langle \Phi_{1\bar{1}} | V_P | \Phi_{2\bar{1}} \rangle = \langle \psi_{200} | V_{P_1} | \psi_{210} \rangle \rightarrow -\frac{3Z_P}{Z_T R^2}, \quad (3.5)$$

where  $Z_T$  is the effective charge of the  $n=2$  hydrogenic orbital. For helium targets, we estimate  $Z_T$  through the energy condition  $-2Z_T^2/2 \times 2^2 = -2^2/2 \times 1^2 + E_L$ ; the peak energy  $E_L \cong 1.3$  and so  $Z_T \cong 1.7$ . It gives a dependence in Eqs. (3.4) and (3.5):  $-Z_P D_M / R^2$  with  $D_0=2$  and  $D_1=1.76$ , which do not differ greatly from the values 2.8 and 2.4, respectively, obtained by Stolterfoth, Brand, and Prost.<sup>7</sup>

In the  $M=0$  subspace, the coupling with the  $2s^2 1S$  state can be neglected in region II, because the difference of energy  $\Delta_{10} = E_1 - E_0 = 0.076$  a.u. and so the phase factor containing such a difference in Eq. (2.28) oscillates, canceling the transitions between Stark levels for  $t > 1/\Delta_{10} = 13$  a.u. This is not the case for the mixing between  $2s2p^1P$  and  $2p^2 1D$ , where such cancellation takes place at much larger time:  $t > 1/\Delta_{12} = 110$  a.u., well within region II.

Factorizing out the Coulomb behavior:  $b_{LM}(\rho, t) = t^{2ia} \exp(-\Gamma_L t/2) c_{LM}(\rho, t)$  [see Eqs. (2.10) and (3.2)] we find that, for  $t \ll \Gamma_L^{-1}$ :  $i\partial/\partial t b_{00}(\rho, t) = i\partial/\partial t b_{22}(\rho, t) = 0$ , and

$$\begin{aligned} i\frac{\partial}{\partial \tau} c_{1M}(\rho, \tau) &= \frac{\lambda_M}{\tau^2} \exp(i\tau) c_{2M}(\rho, \tau), \\ i\frac{\partial}{\partial \tau} c_{2M}(\rho, \tau) &= \frac{\lambda_M}{\tau^2} \exp(-i\tau) c_{1M}(\rho, \tau), \end{aligned} \quad (3.6)$$

where we introduce the variable  $\tau = \Delta_{12}t$ , and  $\lambda_M = \Delta_{12}\beta_M$ , with

$$\beta_0 = -\frac{2\sqrt{3}Z_P}{Z_T v^2}, \quad \beta_1 = -\frac{3Z_P}{Z_T v^2}. \quad (3.7)$$

The system of differential equations can be easily written as two independent differential equations:

$$\frac{d^2 c_1}{d\tau^2} + \left[ \frac{2}{\tau} - i \right] \frac{dc_1}{d\tau} + \frac{\lambda^2 c_1}{\tau^4} = 0, \quad (3.8a)$$

$$\frac{d^2 c_2}{d\tau^2} + \left[ \frac{2}{\tau} + i \right] \frac{dc_2}{d\tau} + \frac{\lambda^2 c_2}{\tau^4} = 0. \quad (3.8b)$$

where, for notational convenience, we omit  $\rho$  and the subscript  $M$ . It is evident that if  $c_1(\tau)$  is a solution of Eq. (3.8a),  $c_2(\tau) = c_1^*(\tau) = c_1(-\tau)$  is a solution of Eq. (3.8b), so we need to concentrate on the former one.

As required by Eq. (2.28), we need to find the following solution:  $\mathbf{c}(\tau) = \mathbf{R}\mathbf{c}(\tau = \infty)$ , where  $\mathbf{R}$  is a unitary matrix. In the  $M=0$  and 1 subspaces, it reads

$$\mathbf{R}_M = \begin{bmatrix} R_{11}(\tau) & \exp(i\tau)R_{12}(\tau) \\ \exp(-i\tau)R_{21}(\tau) & R_{22}(\tau) \end{bmatrix}, \quad (3.9)$$

and is diagonal otherwise. The asymptotic limit requires  $R_{i,j} \rightarrow \delta_{i,j}$ , and the norm conservation that  $\text{Det}\mathbf{R} = 1$ . It is convenient to write  $R_{12}(\tau) = iR'_{12}(\tau)$  and  $R_{21}(\tau) = iR'_{21}(\tau)$ ; so it follows that  $R_{22}(\tau) = R^*_{11}(\tau)$  and  $R'_{21}(\tau) = R'^*_{12}(\tau)$ , and the norm:  $1 = |R'_{11}|^2 + |R'_{12}|^2$ .

### A. Iterative solution

Proposing the following power expansion in terms of the polarization strength  $\lambda$ :

$$\begin{aligned} R_{11}(\tau) &= \sum_n \lambda^{2n} R^{(2n)}(\tau), \\ \exp(i\tau)R'_{12}(\tau) &= \sum_n \lambda^{2n+1} R^{(2n+1)}(\tau), \end{aligned} \quad (3.10)$$

and substituting in Eq. (3.6), it is found that  $R^{(n)}$  satisfy the following relations:

$$\begin{aligned} R^{(2n+1)}(\tau) &= + \int_{\tau}^{\infty} dx \exp(ix) R^{(2n)*}(x)/x^2, \\ R^{(2n)}(\tau) &= - \int_{\tau}^{\infty} dx \exp(ix) R^{(2n-1)*}(x)/x^2. \end{aligned} \quad (3.11)$$

Starting with  $R^{(0)} = 1$ , it follows by integration<sup>12</sup>

$$\mathbf{R} \approx \begin{bmatrix} 1 + \lambda^2 G_{23}^{31}(\tau) + \lambda^2 G_{12}^{21}(-i\tau) + \mathcal{O}(\lambda^4) & \exp(i\tau) \lambda G_{12}^{21}(-i\tau) + \mathcal{O}(\lambda^3) \\ -\exp(-i\tau) \lambda G_{12}^{21}(i\tau) + \mathcal{O}(\lambda^3) & 1 + \lambda^2 G_{23}^{31}(-i\tau) + \mathcal{O}(\lambda^4) \end{bmatrix}. \quad (3.16)$$

In Fig. 1(a), we show the amplitudes  $c_1(\tau)$  and  $c_2(\tau)$  calculated to first order, imposing  $c_2(\tau=2) = 1$  for  $\lambda = -0.264$ , corresponding to the coupling between  $2s2p^1P_0$  and  $2p^2^1D_0$  for  $\text{He}^+$ -He collision at 7-keV impact energy. In Fig. 1(b), we add the real part of the second order [Eq. (3.13)]. As the order increases, oscillation occurs for  $\tau < \lambda$ . Note that, *unless* the infinite orders are included, the norm (dotted line) is violated for small  $\tau$ .

It is interesting to remark that the iterative method here developed can be straightforwardly generalized to any other potential of the type  $1/t^n$ , and for larger systems of equations.

### B. Approximate trigonometric rotation

The exact calculation, as developed in the preceding section, is difficult to treat and very complicated to

$$\begin{aligned} R^{(1)}(\tau) &= \frac{1}{\tau} \exp(i\tau/2) W_{-1,1/2}(-i\tau) \\ &= -i \exp(i\tau) G_{12}^{21}(-i\tau)_{0,-1}, \end{aligned} \quad (3.12)$$

where  $W$  and  $G$  are the Whittaker<sup>13</sup> and Meijers's<sup>14</sup> functions, respectively. The use of the norm conservation equation, to order  $\lambda^2$ , gives

$$\text{Re}(R^{(2)}) = -|W_{-1,1/2}(-i\tau)|^2 / (2\tau^2): \quad (3.13)$$

The full second order can be calculated with the Weyl transformation<sup>15</sup> of  $G_{12}^{21}$ :

$$\begin{aligned} R^{(2)}(\tau) &= G_{23}^{31}(\tau) + i\tau G_{0,-1,-2}^{-2,1} \\ &= \frac{i}{3\tau^3} {}_3F_1(1, 2, 3; 4; i/\tau), \end{aligned} \quad (3.14)$$

and so on. The Meijer's  $G$  functions express a power series in powers of  $\tau$ . Their asymptotic limits are known and produce<sup>16</sup>

$$\begin{aligned} R_{11}(\tau \rightarrow \infty) &= 1 + \lambda^2 [i/(3\tau^3) - 1/(2\tau^4) + \dots] \\ &\quad + \lambda^4 [-1/(18\tau^6) + \dots] + \mathcal{O}(\lambda^6), \\ R'_{12}(\tau \rightarrow \infty) &= \lambda [i/\tau^2 + 2/\tau^3 + \dots] \\ &\quad + \lambda^3 [1/(3\tau^5) + \dots] + \mathcal{O}(\lambda^5), \\ R_{11}(\tau \rightarrow 0) &= 1 - \lambda^2 [1/(2\tau^2)] + \mathcal{O}(\lambda^4), \\ R'_{12}(\tau \rightarrow 0) &= \lambda(1/\tau) + \mathcal{O}(\lambda^3). \end{aligned} \quad (3.15)$$

The manipulation of the series becomes untractable for higher orders in  $\lambda$ . To second order in  $\lambda$  the mixing matrix then reads

proceed to higher orders, which are relevant at short distances. However, a simple approximation can be done for small  $\tau$ . In this case, the main contribution of the integrand of Eq. (3.11) comes from  $x \sim \tau$ , so we can approximate the odd orders by

$$R^{(2n+1)}(\tau) \sim \exp(i\tau) \int_{\tau}^{\infty} dx R^{(2n)*}(x)/x^2, \quad (3.17)$$

By keeping the same expression for the even orders, we find

$$R^{(2n+1)} \sim \exp(i\tau) \frac{(-1)^n}{(2n+1)! \tau^{2n+1}}, \quad (3.18)$$

$$R^{(2n)} \sim \frac{(-1)^n}{(2n)! \tau^{2n}},$$

which can be summed up to all orders to give the well-

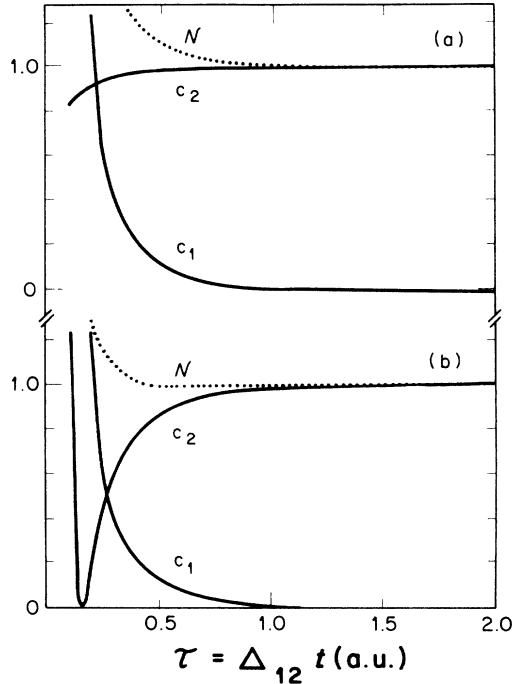


FIG. 1. (a). Amplitudes  $c_1(\tau)$  and  $c_2(\tau)$  calculated to first order with the condition  $c_2(\tau=2)=1$  as a function of  $\tau=\Delta_{12}t$ , for  $\lambda=-0.263$ . It corresponds to the mixing between  $2s2p\ ^1P_0$  and  $2p^2\ ^1D_0$  for  $Z_p=1$  and  $v=0.26$  a.u. (equivalent to  $\text{He}^+-\text{He}$  collision at 7-keV impact energy).  $N$  denotes the norm. (b) Similar to (a), adding the real part of the second order [Eq. (3.13)].

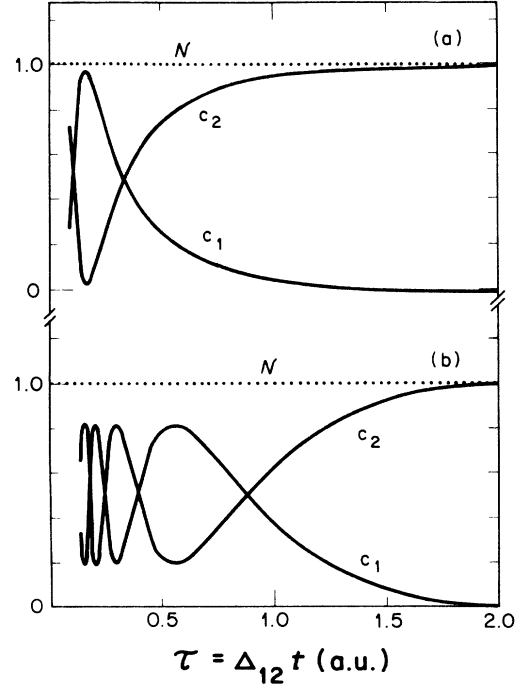


FIG. 2. (a) Amplitudes  $c_1(\tau)$  and  $c_2(\tau)$  calculated with the approximate trigonometric rotation with the condition  $c_2(\tau=2)=1$ , for  $\lambda=-0.263$ . As in Fig. 1, it corresponds to  $Z_p=1$  and  $v=0.26$  a.u. (equivalent to  $\text{He}^+-\text{He}$  at 7-keV impact energy). (b) Similar to (a), for  $\lambda=-0.90$ , corresponding to  $Z_p=1$  and  $v=0.14$  a.u. (these parameters correspond to  $\text{He}^+-\text{He}$  collisions at 2-keV impact energy).

known trigonometric functions

$$R_{11}^{(t)}(\tau)=\cos(\lambda/\tau), \quad R_{12}^{(t)}(\tau)=\sin(\lambda/\tau), \quad (3.19)$$

and so

$$\mathbf{R}^{(t)} = \begin{bmatrix} \cos(\lambda/\tau) & i \exp(i\tau)\sin(\lambda/\tau) \\ i \exp(-i\tau)\sin(\lambda/\tau) & \cos(\lambda/\tau) \end{bmatrix}, \quad (3.20)$$

where the superscript  $(t)$  denotes the trigonometric approximation. The norm is then exactly conserved. At small  $\tau$ , i.e., for  $t < 1/\Delta_{12}$ , the trigonometric rotation is expected to hold: the states can be considered degenerate and the rotation behaves as a usual standard Stark mixing [note that it gives the correct limit as  $\tau \rightarrow 0$ , as compared with Eq. (3.15)]. However, as also expected, the trigonometric rotation becomes less accurate as  $\tau$  increases.

Figs. 2(a) and 2(b) show  $c_1(\tau)$  and  $c_2(\tau)$  for  $\lambda=-0.264$  and  $-0.90$ , corresponding to the couplings between  $2s2p\ ^1P_0$  and  $2p^2\ ^1D_0$  for  $\text{He}^+-\text{He}$  collision at 7- and 2-keV impact energy, respectively, where experiments were carried out.<sup>8,10</sup> Note the trigonometric function depends only on  $\lambda/\tau=\beta/t$ , and retains no trace of the energy difference  $\Delta_{12}$ , which is only present in the exponential of the nondiagonal terms. This factor  $\exp(i\tau)$  introduces oscillations at large  $\tau$ . Note that for  $\tau \geq 0.3$ , the trigonometric approximation [Fig. 29a)] does not differ greatly from the exact second-order approximation to the

real part in  $\lambda^2$  [Fig. 1(b)].

Assuming that the state ends in the  $^1D$ ,<sup>17</sup> the first dip (which corresponds to the first peak of the  $^1P$ ) occurs at  $\beta/t \sim \pi/2$ , replacing  $t$  by  $t_E$  (see the Appendix), we can predict, very roughly, the first effect of the Stark mixing when

$$|E - E_L| \sim \frac{\pi\alpha}{2|\beta_M|}, \quad (3.21)$$

where  $\alpha$  is defined in Eqs. (2.24) and (2.25) above. At this electron energy, the emission pattern should exhibit some trace of  $^1P_0$  as the emitting state. We will come back later to the subject.

In this section we have calculated the exact first order in  $\lambda$  term but higher orders are rather untractable. Alternatively, a trigonometric approximation to all orders is possible which conserves the norm but tends to the correct limit slower than the exact behavior. One way of improving the calculation is to use product of rotations (trigonometric at small and exact one at large  $\tau$ ) matched in the intermediate region, say, around  $\tau \sim \lambda$ .

#### IV. EVALUATION OF MATRIX ELEMENTS

In this section, we deal with the algebra to obtain closed forms of the matrix elements, and in the next section, we resume the relevant expressions for heliumlike targets.

### A. $P$ -matrix elements using the trigonometric rotation

Let us start considering the diagonal terms

$$P_{LM,LM}^{(t)} = \int_0^\infty dt \exp(-\omega_{LM}t) t^{i\alpha} D^{-*}(a', \mathbf{v}', -\mathbf{v}t) \times \cos(|\beta_M|/t), \quad (4.1)$$

where, for a reason that will become evident later, we write  $\alpha$  instead of  $a$ . In the forward direction,  $|A'/\omega_{LM}| \ll 1$ ,  $D^{-*}(a', \mathbf{v}', -\mathbf{v}t)$  transforms into the Coulomb factor [see Eq. (2.9)] which is independent of  $t$ , and so Eq. (4.1) becomes a simple Laplace transform. Thus the integral is given in closed form<sup>18</sup> in terms of the Bessel function  $K_{-1-i\alpha}$  which can be related to the hypergeometric function  $U$ .<sup>19</sup> After some algebra we find

$$P_{LM,LM}^{(t)} = [\Gamma(1-ia') \exp(\pi a'/2)] B_{LM} \frac{1}{\omega_{LM}} C_{LM}^{(t)}, \quad (4.2)$$

$B_{LM}$  is the binding factor [see Eq. (2.16)],

$$C_{LM}^{(t)} = \frac{1}{2U_0} [\exp(-z_{(+)}) U_{(+)} + \exp(-z_{(-)}) U_{(-)}], \quad (4.3)$$

$$U_0 = \lim_{\varepsilon \rightarrow 0} U(-1/2 - i\alpha, -1 - 2i\alpha, \varepsilon) = \frac{\Gamma(2+2i\alpha)}{\Gamma(3/2+i\alpha)}, \quad (4.4)$$

$$U_{(+,-)} = U(-1/2 - i\alpha, -1 - 2i\alpha, 2z_{(+,-)}), \quad (4.5)$$

$z_{(+,-)} = (2|\beta_M|\omega_{LM})^{1/2}(1 \pm i)$ , and  $\alpha = a$ . Once again we use the superscript  $(t)$  to indicate that the calculation was done within the trigonometric approximation. On the other hand, at large angles, when  $|A'/\omega_{LM}| \gg 1$ ,  $D^{-*}(a', \mathbf{v}', -\mathbf{v}t) \sim (A't)^{-ia}$  [see Eq. (2.9)] and so the integral remains basically the same with  $\alpha = a - a'$ . The result is then

$$P_{LM,LM}^{(t)} = \left[ \frac{\Gamma(1-i\alpha)}{\Gamma(1+ia)} \left( \frac{A'}{\omega_{LM}} \right)^{-ia'} \right] B_{LM} \frac{1}{\omega_{LM}} C_{LM}^{(t)}. \quad (4.6)$$

The terms in square brackets of Eqs. (4.2) and (4.6) correspond to the limits of the focusing factor  $F_{LM}$  [see Eq. (2.18)]. Then, we approximate

$$P_{LM,LM}^{(t)} = F_{LM} B_{LM} \frac{1}{\omega_{LM}} C_{LM}^{(t)} = P_{LM} C_{LM}^{(t)} \quad (4.7)$$

for all angles, where  $F_{LM}$  is given by Eq. (2.17). The parameter  $\alpha$ , which contains both long-distance interactions, is defined in Eqs. (2.24) and (2.25). As indicated before, in our energy range of interest,  $a \gg a'$  and so  $\alpha = a$  with a good accuracy.

For the nondiagonal profile matrix terms, we should solve the same kind of integral (4.1) with  $i \sin(\beta_M/t)$  instead of  $\cos(\beta_M/t)$ . Following the same technique, we find after some algebra

$$P_{KM,LM}^{(t)} = -i F_{LM} B_{LM} \frac{1}{\omega_{LM}} S_{LM}^{(t)} = -i P_{LM} S_{LM}^{(t)}, \quad (4.8)$$

where  $|K-L|=1$  and

$$S_{LM}^{(t)} = \frac{i}{2U_0} [\exp(-z_{(+)}) U_{(+)} - \exp(-z_{(-)}) U_{(-)}], \quad (4.9)$$

with  $\alpha$  defined in Eq. (2.25). The negative sign in Eq. (4.8) takes into account the  $\text{sgn}(\beta_M) = -1$ . Note that  $z_{(+,-)}$  is a function of  $|\beta_M|$ , and so the real part of  $z_{(+,-)}$  is positive, as required by the integration procedure.<sup>18</sup> We conclude that the profile matrix elements can be written as a product of four factors: unperturbed shape, binding, focusing, and the new terms  $C_{LM}^{(t)}$  and  $S_{LM}^{(t)}$  which take into account the Stark mixing.

Finally, we can write the trigonometric profile matrix as

$$\mathbf{P}^{(t)} = \begin{pmatrix} P_{00} & 0 & 0 & 0 & 0 & 0 \\ 0 & P_{10} C_{10}^{(t)} & -i P_{20} S_{20}^{(t)} & 0 & 0 & 0 \\ 0 & -i P_{10} S_{10}^{(t)} & P_{20} C_{20}^{(t)} & 0 & 0 & 0 \\ 0 & 0 & 0 & P_{11} C_{11}^{(t)} & -i P_{21} S_{21}^{(t)} & 0 \\ 0 & 0 & 0 & -i P_{11} S_{11}^{(t)} & P_{21} C_{21}^{(t)} & 0 \\ 0 & 0 & 0 & 0 & 0 & P_{22} \end{pmatrix}. \quad (4.10)$$

It should be pointed out that  $P_{LM} = P_L$ , i.e., independent of the magnetic quantum number, because  $F_{LM} = F_L$ ,  $B_{LM} = B_L$ , and  $\omega_{LM} = \omega_L$ . Only  $C_{LM}^{(t)}$  and  $S_{LM}^{(t)}$  depend on  $M$ .

The Sommerfeld parameters  $a$  and  $a'$  take into account the Coulomb interactions, and  $\beta_M$  is the strength of the

polarization potential. The three correcting factors to the unperturbed distribution:  $F_{LM}$ ,  $B_{LM}$ , and  $C_{LM}^{(t)}$  (or  $S_{LM}^{(t)}$ ) depend primarily on  $a'$ ,  $a$ , and  $\beta_M$ , respectively, being unity as the corresponding parameter is switched off; i.e.,  $F_{LM}(a'=0) = B_{LM}(a=0) = C_{LM}^{(t)}(\beta_M=0) = 1$ . In addition, as  $\beta_M \rightarrow 0$ ,  $S_{LM}^{(t)} \rightarrow 0$  and the profile matrix tends to

be diagonal. The integration technique here developed is quite accurate:  $P^{(t)}$ -matrix elements are correct solutions of Eq. (4.1) when  $\theta=0$ , very reliable for very large  $\theta$ , and it has the correct limit for all angles as  $\beta \rightarrow 0$ .

Figures 3(a) and 3(b) display in solid lines the real parts of  $S_{20}^{(t)}$  and  $C_{20}^{(t)}$  (the imaginary parts are small) for a point projectile of unity charge impinging on He target at  $v=0.1414$  (corresponding to 2-keV He<sup>+</sup> impact energy on helium) as a function of the ejected electron energy. The functions  $C_{LM}^{(t)}$  and  $S_{LM}^{(t)}$  behave quite like the trigonometric functions cosine and sine, respectively, as can be seen by expanding by a power series the trigonometric functions in Eq. (4.1). For  $\alpha \gg 1$ , we can approximate, crudely,

$$\begin{aligned} S_{LM}^{(t)} &\sim \sin \left[ \frac{|\beta_M| \omega_{LM}}{i\alpha} \right], \\ C_{LM}^{(t)} &\sim \cos \left[ \frac{|\beta_M| \omega_{LM}}{i\alpha} \right]. \end{aligned} \quad (4.11)$$

In Fig. 3, we also show in dashed lines these simple expressions which follow the more precise calculations using Eqs. (4.3) and (4.9). The influence of the nondiagonal terms will be maximum when the argument of the sine functions is  $\pi/2$ , which is a condition already found in Eq. (3.21).

#### B. P-matrix elements using the exact first order

To calculate the first order in  $\beta_M$ , obtained with the iterative method, we need to evaluate the integral (4.1) containing  $\lambda G_{12}^2(-i\tau|_{0,-1}^{-1})$  instead of  $\cos(\beta_M/t)$ . Following the same pattern as before, it is found that the profile matrix has a similar structure to Eq. (4.10), given by

$$\mathbf{P} = \begin{pmatrix} P_{00} & 0 & 0 & 0 & 0 & 0 \\ 0 & P_{10}C_{10,10} & -iP_{20}S_{10,20} & 0 & 0 & 0 \\ 0 & -iP_{10}S_{20,10} & P_{20}C_{20,20} & 0 & 0 & 0 \\ 0 & 0 & 0 & P_{11}C_{11,11} & -iP_{21}S_{11,21} & 0 \\ 0 & 0 & 0 & -iP_{11}S_{21,11} & P_{21}C_{21,21} & 0 \\ 0 & 0 & 0 & 0 & 0 & P_{22} \end{pmatrix}. \quad (4.12)$$

To first order in  $\beta_M$  we have  $C_{LM,LM}^{(1)}=1$ , and the nondiagonal elements read<sup>20,21</sup>

$$\begin{aligned} S_{KM,LM}^{(1)} &= |\beta_M| \frac{\omega_{LM}}{i\alpha(1+i\alpha)} \\ &\times {}_2F_1 \left[ 1, i\alpha, 2+i\alpha, 1+i \frac{\Delta_{KL}}{\omega_{LM}} \right], \end{aligned} \quad (4.13)$$

where  $\Delta_{LK} = E_L - E_K$ . In Fig. 3(a) we plot in a solid line

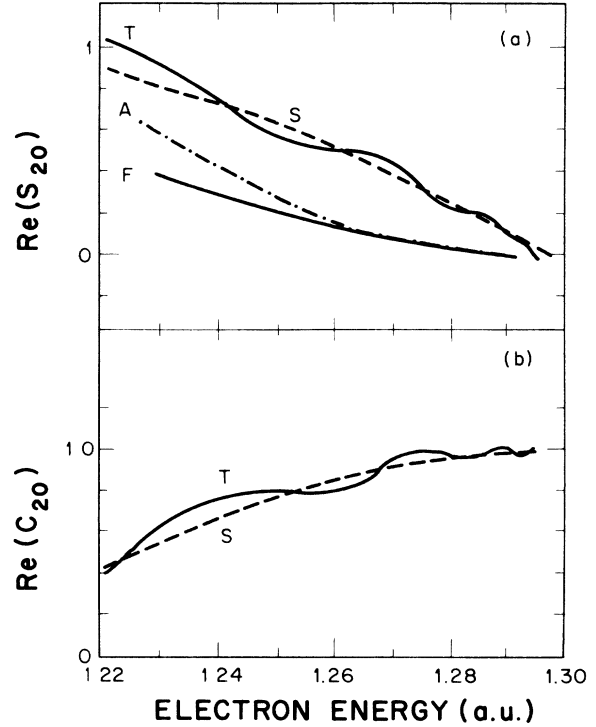


FIG. 3. (a) Real part of  $S_{20}$  as a function of the electron energy in atomic units in the forward direction, corresponding to projectiles with unit charge impinging on He target at  $v=0.1414$  (or 2-keV He<sup>+</sup> on He). Curves denoted with T and S correspond to Eqs. (4.9) and (4.11), respectively. Curves F and A denote the real parts of  $S_{10,20}$  corresponding to Eqs. (4.13) and (4.16), respectively. (b) Similar to (a). Curves T and S denote the real parts of  $C_{20}^{(t)}$  given by Eqs. (4.3) and (4.11), respectively.

the real part of  $S_{10,20}^{(1)}$  (the imaginary part here is not negligible) and compare with the previous results. Two limits of Eq. (4.13) will be discussed next.

For electron energies larger than the difference of energies, i.e.,  $|E - E_{1,2}| > \Delta_{12} \sim 0.25$  eV, i.e., in the tails of the peak, the argument of the hypergeometric function is almost unity, and so Eq. (4.13) can be approximated by

$$S_{KM,LM}^{(1)} \sim \frac{|\beta_M| \omega_{LM}}{i\alpha} \sim \frac{3}{vZ_T} [E_L - E - i\Gamma_L/2] \quad \text{for } \omega_{LM} \gg \Delta_{LK} \quad (4.14)$$

which is the result that we would obtain if the first order of the trigonometric rotation were used [compare with the first order in  $\beta_M$  of  $S_{LM}^{(1)}$  in Eq. (4.11)]. This limit is expected, since for  $t \leq 1/\Delta_{12}$ , the trigonometric rotation holds, and this region maps into the electron peak tail. Based on the *approximate* relation (4.14), we are able to infer some features of the influence of the nondiagonal terms. It is then expected that the Stark mixing far from the peak does not depend on  $Z_p$ , it increases as  $\nu$  decreases and it depends linearly on  $|E_L - E|$ . Also note that for most of the experimental situations,  $S_{KM,LM}^{(1)} < 1$ .

On the other hand, for energies satisfying  $|E - E_{1,2}| < \Delta_{12}$ , i.e., near the resonant energy, deviations from Eq. (4.14) are expected, which are related to the fact that the trigonometric rotation breaks down at large collision times. In this case  $\omega_{LM} \ll \Delta_{LK}$ , and after performing a Kummer's transformation to the hypergeometric function in Eq. (4.13), we find that

$$S_{KM,LM}^{(1)} \sim \frac{|\beta_M| \omega_{LM}^2}{\Delta_{KL} \alpha (i\alpha - 1)}, \quad \text{for } \omega_{LM} \ll \Delta_{LK}, \quad (4.15)$$

which happens to be the Laplace transformation of the asymptotic limit as  $t \rightarrow \infty$  of the first order of the nondiagonal rotation element [ $R'_{12}$  in Eq. (3.15)].

To estimate higher orders, we could combine the exact first order with the one using the trigonometric rotation for higher order by including the behavior of the first order near the resonant energy within the argument of the function sine, as follows:

$$S_{KM,LM} \sim \sin \left[ \frac{|\beta_M| \omega_{LM}^2}{\alpha [i\omega_{LM} + \Delta_{KL} (i\alpha - 1)]} \right]. \quad (4.16)$$

This simple expression gives a good account of the first order and the trigonometric approximation near and far off the resonant energy, respectively, as shown in Fig. 3(a). There are no major changes to curve  $S$  in Fig. 3(b) if we approximate  $C_{LM,LM}$  by the cosine of the same argument of Eq. (4.16).

### C. Calculation of the terms $y_{LM}$

If the final state of the electron which remains bound to the target is spherical symmetric, such as for the  $K$  shell,  $y_{LM}$  reads

$$\begin{aligned} y_{LM} &= \langle \Phi_f | 1/r_{12} | \Phi_{LM} \rangle \\ &= \pm (-i)^L e^{i\kappa_L} \left[ \frac{\Gamma_L}{2\pi\sqrt{2E}} \right]^{1/2} Y_L^{\bar{M}}(\Omega), \end{aligned} \quad (4.17)$$

where by the symmetry property used in Sec. III we have  $Y_L^{\bar{M}} = [Y_L^{-M} + (-1)^M Y_L^M] / \sqrt{2}$  for  $M \neq 0$  ( $Y_L^0 = Y_L^0$ ),  $\Omega \equiv (\theta, \phi = 0)$  is the solid angle of the ejected electron, and

$$\kappa_L = \arg \Gamma(L + 1 - i/\sqrt{2E}). \quad (4.18)$$

It is important to pay attention to the phase factor, which corresponds to the one of the continuum states, because it plays an important role in the interference between two states with equal magnetic quantum number

$M$  and different orbital one  $L$ . Further, as the sign of the Slater integral (the one involving the real radial functions) is not generally available, there is an uncertainty<sup>22</sup> on the sign as indicated in the equation above. This uncertainty can be removed by inspecting the sign of the matrix element used in the calculation of the width  $\Gamma_L$ .

### V. EXPLICIT EXPRESSIONS FOR He TARGETS

The theoretical double differential cross sections read

$$\frac{d\sigma}{d\Omega dE} = \sum_{j,k} U_{j,k} D_{j,k} = \text{Tr}(\mathbf{U}^t \cdot \mathbf{D}), \quad (5.1)$$

$$U_{j,k} = \sqrt{2E} \left[ \sum_n y_n P_{n,j} \right]^* \left[ \sum_m y_m P_{m,k} \right]. \quad (5.2)$$

For the Auger transition  $\text{He}^{**}(n=2) \rightarrow \text{He}(1s) + e$ , we can reduce the expression of the terms of the matrix  $U$  to

$$\begin{aligned} U_{00,00} &= \frac{|P_0|^2}{2\pi} |\sqrt{\Gamma_0} Y_0^0|^2, \\ U_{22,22} &= \frac{|P_2|^2}{2\pi} |\sqrt{\Gamma_2} Y_2^{\bar{2}}|^2, \\ U_{1M,1M} &= \frac{|P_1|^2}{2\pi} |(\mp i) e^{i\kappa_1} \sqrt{\Gamma_1} Y_1^{\bar{M}} C_{1M,1M} \\ &\quad + (\pm i) e^{i\kappa_2} \sqrt{\Gamma_2} Y_2^{\bar{M}} S_{2M,1M}|^2, \\ U_{2M,2M} &= \frac{|P_2|^2}{2\pi} |(\mp 1) e^{i\kappa_2} \sqrt{\Gamma_2} Y_2^{\bar{M}} C_{2M,2M} \\ &\quad + (\mp 1) e^{i\kappa_1} \sqrt{\Gamma_1} Y_1^{\bar{M}} S_{1M,2M}|^2, \\ U_{1M,2M} &= \frac{P_1^* P_2}{2\pi} [(\mp i) e^{i\kappa_1} \sqrt{\Gamma_1} Y_1^{\bar{M}} C_{1M,1M} \\ &\quad + (\pm i) e^{i\kappa_2} \sqrt{\Gamma_2} Y_2^{\bar{M}} S_{2M,1M}]^* \\ &\quad \times [(\mp 1) e^{i\kappa_2} \sqrt{\Gamma_2} Y_2^{\bar{M}} C_{2M,2M} \\ &\quad + (\mp 1) e^{i\kappa_1} \sqrt{\Gamma_1} Y_1^{\bar{M}} S_{1M,2M}], \end{aligned} \quad (5.3)$$

where  $M=1,2$ ,  $U_{2M,1M} = U_{1M,2M}^*$ , and zero otherwise. The upper and lower signs in Eq. (5.3) correspond to the sign of the Slater integral. The profile terms  $P_L$  do not depend on  $M$  and are given by

$$P_L = F_L B_L \frac{1}{\frac{\Gamma_L}{2} + i(E_L - E)}, \quad (5.4)$$

where  $B_L$  and  $F_L$  are the binding and focusing factors defined in Eqs. (2.16) and (2.17), respectively.

The functions which account for the Stark mixing are  $C_{LM,LM}$  and  $S_{KM,LM}$  and they are quite similar to the functions cosine and sine, respectively.  $C_{LM,LM}$  was calculated in the trigonometric rotation to give  $C_{LM}^{(1)}$  [see Eq. (4.3)] and it is well represented by the simple cosine function Eq. (4.11) [see Fig. 3(b)]. On the other hand,  $S_{KM,LM}$  was calculated in first perturbative order [Eq. (4.13)], in the trigonometric approximation [Eq. (4.9)], and it can also be approximated by a simple sine function as shown

in Eqs. (4.11) and (4.16). This latter expression gives also a good estimation of both limits as shown in Fig. 3(a). Although in the present work we perform full calculations, we like to remark that those simple expressions, such as Eqs. (4.11) and (4.16), contain the basic physics of the problem, and so the computation of the hypergeometric function  $U$  and  ${}_1F_1$  can be avoided.

How we address the normalization property of the elements  $U_{LM,LM}$ . After integrating on the energy and angular distributions, we find

$$\int dE \int d\Omega U_{LM,LM} \sim 1 + (\Gamma_K - \Gamma_L) \left| \frac{\beta_M}{2\alpha} \right|^2, \quad (5.5)$$

where we have assumed that the focusing effect does not modify greatly the norm<sup>6</sup> and

$$|C_{LM,LM}|^2 + |S_{KM,LM}|^2 = 1. \quad (5.6)$$

For most of the cases here studied, the norm can be considered unity within a few percent.

## VI. RESULTS

To compare with the experimental double differential cross section in energy and angular distribution of the ionized electron, we simply have to replace the density-matrix elements in Eq. (2.29), and convolute with the experimental resolution  $f$ , to give

$$\frac{d\sigma}{d\Omega dE} = \sum_{j,k} U'_{j,k} D_{j,k} = \text{Tr}(U'^t \cdot \mathbf{D}), \quad (6.1)$$

$$U'_{j,k} = \int dE' f(\eta|E - E') U_{j,k}(E'), \quad (6.2)$$

$\eta$  being the energy acceptance of the apparatus. Since  $f$  is a real function, then  $U_{j,k} = U_{k,j}^*$ . For simplicity, we here consider an ideal detector where  $f(\eta|E - E') = \delta(E - E')$  and so  $U'_{j,k} = U_{j,k}$ . Equation (6.1) also allows us to consider the inverse problem, that is, to find the density-matrix elements from a given set of experimental data. For the case here studied, the Hermitian matrix  $\mathbf{D}$  is determined in general by 14 independent parameters: 6 diagonal (real:  $D_{00,00}$ ,  $D_{1M,1M}$ ,  $D_{2M,2M}$ ) and 4 nondiagonal (complex:  $D_{00,10}$ ,  $D_{00,20}$ ,  $D_{10,20}$ ,  $D_{11,21}$ ). If we neglect the overlap with the  $2s^2\ ^1S$ , the number of parameters reduces to 10. Furthermore, if, as usual,<sup>10</sup> it is assumed that Eq. (6.1) can be expressed as a modulus square of a complex sum, we can then write

$$D_{j,k} \sim \sqrt{D_{j,j} D_{k,k}} \exp[i(\varphi_k - \varphi_j)], \quad (6.3)$$

and the number of parameters is brought to 8. Most of the experiments only deal with the diagonal density-matrix terms,<sup>8</sup> and a few others<sup>9,10</sup> let us obtain the nondiagonal ones, assuming the approximation above.

For instance, consider the contribution of the subspace  $M=0$  of Eq. (6.1):

$$\begin{aligned} \frac{d\sigma}{d\Omega dE}(M=0) &= U_{10,10} D_{10,10} + U_{20,20} D_{20,20} \\ &+ U_{10,20}^{(R)} \text{Re}(D_{10,20}) \\ &+ U_{10,20}^{(I)} \text{Im}(D_{10,20}), \end{aligned} \quad (6.4)$$

where  $U_{10,20}^{(R)} = 2 \text{Re}(U_{10,20})$  and  $U_{10,20}^{(I)} = -2 \text{Im}(U_{10,20})$ . These terms factorize the off-diagonal density-matrix elements, while  $U_{10,10}$  and  $U_{20,20}$  modulate the diagonal elements or cross sections.

In Fig. 4, we plot the nondiagonal terms  $U_{10,20}^{(R)}$  and  $U_{10,20}^{(I)}$  as a function of the electron energy at  $0^\circ$  and  $180^\circ$  (solid and dashed lines, respectively), corresponding to 2-keV  $\text{He}^+$ -He collision using the first-order theory (similar results are obtained if the trigonometric Stark rotation is used instead). Three features of the *nondiagonal* terms  $U$  should be pointed out: first, for a given angle, they oscillate around the peak, and should account for the interference patterns observed in some experiments<sup>10</sup> (due to the rapid oscillations, its structure should be sensitive to the experimental resolution  $\eta$ ). Second, these nondiagonal terms  $U$  may have some influence in the forward-backward discrepancy,<sup>7</sup> depending on the values of the off-diagonal density-matrix elements. And third, integrating on the energy distribution, we find that, for a given angle, their contributions are comparatively negligible, that is,

$$\int dE' U_{10,20}^{(R,I)} \ll \int dE' U_{L0,L0}, \quad L=1,2. \quad (6.5)$$

It follows that

$$\frac{d\sigma}{d\Omega}(M=0) \cong U_{10,10} D_{10,10} + U_{20,20} D_{20,20} \quad (6.6)$$

and so the procedure developed by Bordenave-Montesquieu, Gleizes, and Benoit-Cattin<sup>8</sup> to obtain total

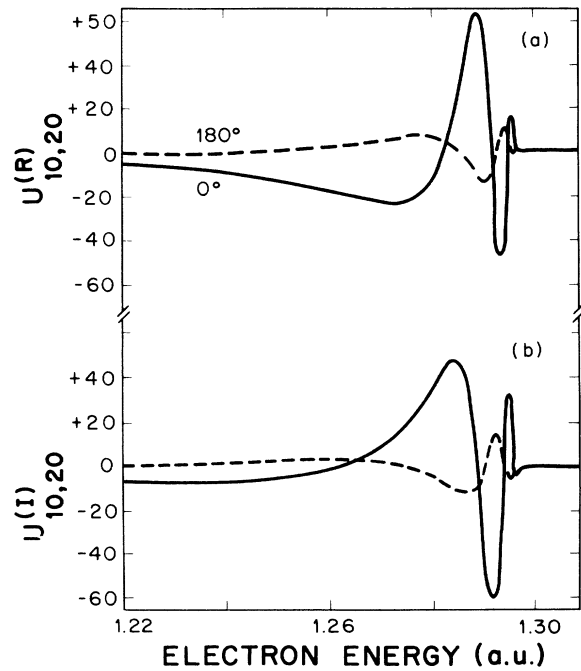


FIG. 4. Nondiagonal terms  $U_{10,20}^{(R)}$  and  $U_{10,20}^{(I)}$  as a function of the energy of the ejected electron. All quantities in atomic units. Calculations were carried out using the first order in the polarization strength. Solid and dashed lines are the results for  $0^\circ$  and  $180^\circ$ , respectively. The parameters correspond to  $Z_p = 1$  and  $v = 0.14$  a.u. (or  $\text{He}^+$ -He collision at 2-keV impact energy).

cross sections from the angular distributions is substantiated.

In Fig. 5, we display the diagonal  $U_{20,20}$  for the same case as Fig. 4, calculated with the first-order [Fig. 5(a)] and trigonometric rotation [Fig. 5(b)]. Different signs for  $L=1$  and  $2$  were used in Eq. (4.18). If equal signs are used instead the spectra at  $\theta=0$  and  $\pi$  exchange roles. It should be remarked that if Stark mixing is switched off, then  $U_{LM,LM}(\theta=0)$  and  $U_{LM,LM}(\theta=\pi)$  differ little, the only source of deviation being the focusing effect, which is a factor almost independent of the electron energy. Thus the differences are due mainly to the influence of the polarization potential. Near the peak energy, long-distance amplitudes are mapped, and so the first order as plotted in Fig. 5(a) is supposed to be more appropriate. As we move to the tail of the distribution, the first order breaks down and the trigonometric rotation should take over. Further, the structures observed in Fig. 5(b) can be related to the amplitudes as a function of time [Fig. 2(b)].

Figure 6 shows the *diagonal* terms  $U_{20,20}$  at  $30^\circ$  and  $150^\circ$  for  $\nu=0.24$  and  $Z_p=1$ , corresponding to 10-keV  $\text{Li}^+$  on helium calculated in first order [Fig. 6(a)] and with the trigonometric rotation [Fig. 6(b)]. Different signs for  $L=1$  and  $2$  were used in Eq. (4.17) in order to fit the data. The theories follow the tendency of the ex-

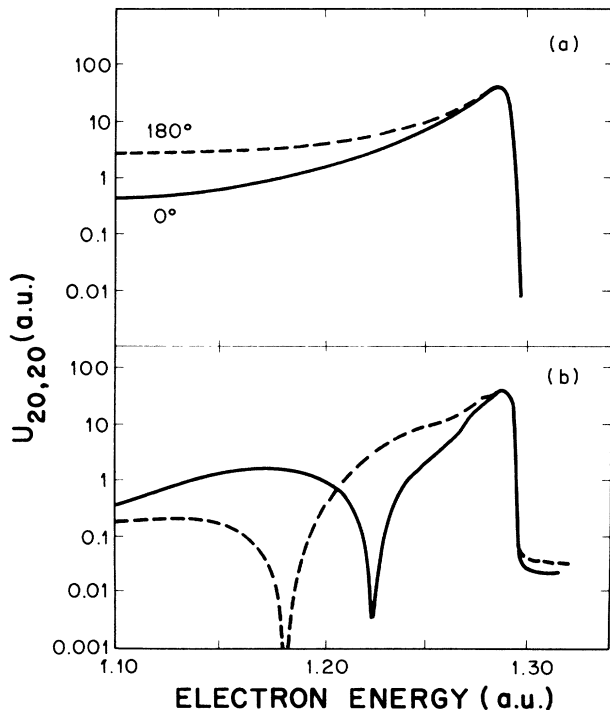


FIG. 5. The diagonal term  $U_{20,20}$  as a function of the energy of the ejected electron. All quantities in atomic units. Calculations were carried out using the first order in the polarization strength (a), and trigonometric rotation (b). Solid and dashed lines are the results for  $0^\circ$  and  $180^\circ$ , respectively. Results at  $180^\circ$  are multiplied by 3.88 and 3 in (a) and (b), respectively, to have equal intensity at the maximum. These factors account mainly for focusing effects. The parameters correspond to  $Z_p=1$  and  $\nu=0.14$  a.u. (or  $\text{He}^+$ -He collision at 2-keV impact energy).

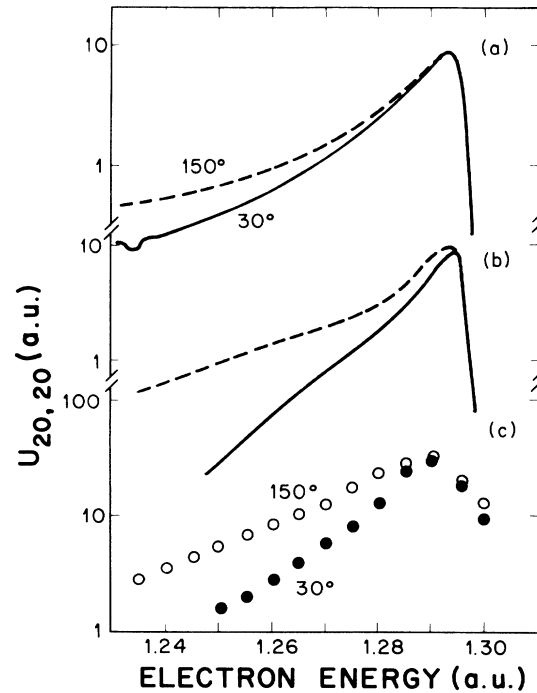


FIG. 6.  $U_{20,20}$  at  $30^\circ$  and  $150^\circ$  for  $Z_p=1$  and  $\nu=0.24$  a.u. (corresponding to 10-keV  $\text{Li}^+$  on He) as a function of the electron energy. All quantities in atomic units. (a) shows the spectra using the first order, (b) displays the results using the trigonometric rotation, and (c) the entire experiment (Ref. 7) in arbitrary units.

periments<sup>7</sup> [Fig. 6(c)]. As indicated in Ref. 7, if  $\theta$  is small, only  $M=0$  is the dominant magnetic sublevel and  $L=2$  is the more likely to be populated via double-promotion rotational coupling. So, the comparison of  $U_{20,20}$  with the entire experiment is quite reasonable. For a more detailed comparison with the data we need to convolute the theoretical results with the instrument resolution and consider kinematic effects which broaden the peak.

In order to study the forward-backward asymmetry of the diagonal terms  $U_{LM,LM}$ , let us define the ratio

$$\mu_{LM}(\theta) = \frac{U_{LM,LM}(\theta)}{U_{LM,LM}(\pi-\theta)}. \quad (6.7)$$

In Fig. 7, we plot  $\mu_{20}(150^\circ)$  for the case of Fig. 6. First order (curve  $F$ ), trigonometric rotation (curve  $T$ ) and the model developed in Ref. 7 (curve  $SBP$ ) are plotted and compared with the experimental ratio. All the theories agree qualitatively with the tendency of the data.

We can *roughly* evaluate  $\mu_{20}$ , by approximating Eq. (6.7) to first order on the nondiagonal matrix  $P$  terms as

$$\mu_{20}(0) \sim \gamma(a') \frac{1 + 2 \text{Im}[\xi_{10,20}(0)S_{10,20}]}{1 + 2 \text{Im}[\xi_{10,20}(\pi)S_{10,20}]} + O(S_{10,20}^2), \quad (6.8)$$

where  $\gamma(a') = 2\pi a' / (1 - e^{2\pi a'})$  is the modulus squared of the Coulomb factor, and

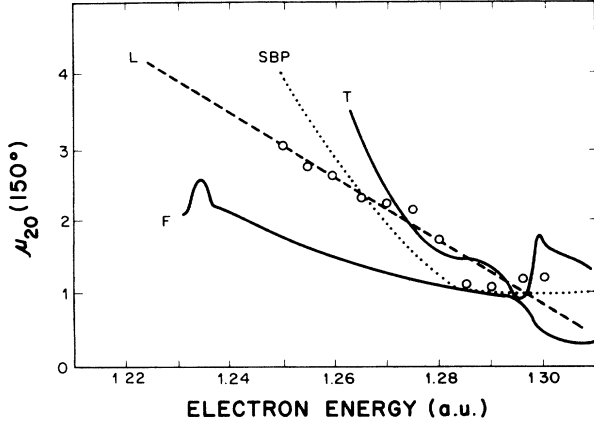


FIG. 7. Asymmetry factor  $\mu_{20}^{-1}(30^\circ) = \mu_{20}(150^\circ)$  as a function of the electron energy in atomic units for  $Z_P = 1$  and  $\nu = 0.24$  (corresponding to 10-keV  $\text{Li}^+$  on He). Solid lines labeled with  $F$  and  $T$  correspond to the first order and trigonometric rotation, respectively. The dashed line denoted by  $L$  corresponds to the linear approximation [Eq. (6.11)]. The dotted line denoted by  $SBP$  and circles is the theory and experiment of Stolterfoth, Brandt, and Prost (Ref. 7), respectively.

$$\xi_{10,20}(\theta) = \frac{y_{10}(\theta)}{y_{20}(\theta)} = \pm (-0.35 + 1.127i) \frac{\cos(\theta)}{3 \cos^2(\theta) - 1}. \quad (6.9)$$

We keep the uncertainty of the sign coming from Eq. (4.18): the upper sign (+) if both Slater integrals corresponding to  $L = 0$  and 1 have the same sign, and the lower sign (-) otherwise. After assuming that the nondiagonal terms of the profile matrix are both *small*, and expressible by the approximation (4.14), we conclude that

$$\mu_{20}(0) \sim \gamma(a') \left[ 1 \mp \frac{2.2\beta_0}{\alpha} (E_2 - E) \right], \quad (6.10)$$

where we restore the sign to  $\beta_0$ :  $\beta_0 < 0$ , if  $Z_P > 0$ . The picture of Eq. (6.10) is simple:  $\gamma(a')$  represents the enhancement in the forward direction due to the projectile focusing, and the correction term in the large parentheses is due to Stark mixing. Energies near the resonant energy  $E \approx E_2$  correspond to long time where there is no mixing and so the Stark correction is null. As we decrease in the energy of the ejected electron, we are mapping smaller times where the Stark mixing populates the  $^1P_0$ . This state provides an angular distribution proportional to  $y_{10} \sim \cos\theta$  enhancing the forward direction and depleting the backward one, or vice versa [depending on the relative phase of Eq. (4.17)]. As mentioned before, the competing effects between the polarization and Coulomb potentials are expressed by the ratio  $\beta_0/\alpha = -2\sqrt{3}/(Z_P\nu)$ . Within this rough approximation, this ratio is independent of  $Z_P$ .

At any other small angle, but larger than the focusing angle, the Coulomb factor can be dropped and the forward-backward ratio can be approximated to be

$$\mu_{20}(\theta) \sim 1 \mp \frac{4.4\beta_0}{\alpha} \frac{\cos(\theta)}{3 \cos^2(\theta) - 1} (E_2 - E). \quad (6.11)$$

The good agreement of this simple approximation with the experiments, as shown in Fig. 7, is better than expected. Equations (6.10) and (6.11) should be understood as very approximate expressions.

Near  $\theta = 54^\circ$ , i.e., when  $y_{20} = 0$  [where Eq. (6.11) is no longer valid], the only emitting source in the  $M = 0$  subspace is  $^1P_0$  which can be populated either by direct collision in region I, or by Stark mixing with  $^1D_0$  in region II. Anyway, we should have in mind that at angles not necessarily very large, the  $M = 2$  subspace dominates the spectrum since  $D_{22,22}$  is found to be much larger than  $D_{20,20}$ .<sup>17</sup> Similar analysis can be made for the  $M = 1$  subspace.

In summary, we have developed a general formalism to calculate the electronic profiles corresponding to autoionizing states, including binding, focusing, and Stark mixing of the close lying states. Attention was paid to the mixing of the  $2s2p\ ^1P$  and  $2p^2\ ^1D$  states of helium target. The influence of the diagonal and nondiagonal elements of the matrices  $R$ ,  $P$ , and  $U$  were studied. The Stark mixing was found to produce forward-backward asymmetry, depending on the signs of the Slater integrals. This uncertainty is removed if also the sign of the Slater integral is available, more than the absolute value. In the subspace  $M = 0$ , we obtain an asymmetry qualitatively in accordance with the available data. More experimental results are needed to test further the present formalism.

#### ACKNOWLEDGMENTS

We would like to thank I. Cordrey for a critical reading of the manuscript. This research has been sponsored by the U.S. Department of Energy, under Contract No. DE-AC05-84OR21400 with Martin Mareitta Energy Systems, Inc.

#### APPENDIX

Neglecting Stark mixing, the diagonal  $P$ -matrix elements are reduced to

$$P_{LM,LM} = P_L \sim \int_0^\infty dt \exp(-\omega_L t) t^{i\alpha} = \frac{\Gamma(1+i\alpha)}{\omega_L^{1+i\alpha}}, \quad (A1)$$

where  $\alpha$  is defined in Eq. (2.24), and  $\omega_L = \Gamma_L / 2 + i(E_L - E)$ . We are interested here in finding where the maximum contribution to  $P_{LM,LM}$  comes from. By examining the integrand, we find that relevant times are around  $t_E \sim i\alpha/\omega_L$ . In the tail of the profile, i.e.,  $E_L - E > \Gamma_L/2$ ,  $t_E$  is real and simply reads

$$t_E \sim \frac{\alpha}{E_L - E} \quad \text{for } E_L - E > \Gamma_L/2. \quad (A2)$$

One example of this relation is Eq. (2.26). Equation (A2) relates the electron profile at a given energy  $E$  with the behavior of the collisional amplitudes at  $t_E$ . The use of the stationary-phase approximation in the vicinities of  $t_E$  gives Eq. (A1) except that the  $\Gamma$  function is approximated by the Stirling formula.

- \*On leave from Instituto de Astronomia y Fisica del Espacio, Casilla de Correo 67, Sucursal 28, 1428 Buenos Aires, Argentina.
- <sup>1</sup>C. Cohen-Tannoudji, B. Diu, and F. Laloe, *Quantum Mechanics* (Wiley, New York, 1977), Vol. 2.
- <sup>2</sup>N. Stolterfoth, Rep. Prog. Theor. Phys. **146**, 315 (1987), and references within.
- <sup>3</sup>R. B. Baker and H. B. Berry, Phys. Rev. **151**, 14 (1966).
- <sup>4</sup>A. Z. Devdariani, V. W. Ostroskii, and Yu. N. Sebayakin, Zh. Eksp. Teor. Fiz. **73**, 412 (1977) [Sov. Phys.—JETP **46**, 215 (1977)].
- <sup>5</sup>J. K. Swenson, C. C. Havener, N. Stolterfoth, K. Sommer, and F. W. Meyer, Phys. Rev. Lett. **63**, 35 (1989).
- <sup>6</sup>R. O. Barrachina and J. H. Macek, J. Phys. B **22**, 2151 (1989). See also M. Yu. Kuchiev and S. A. Sheinerman, J. Phys. B **21**, 2077 (1988).
- <sup>7</sup>N. Stolterfoth, D. Brand, and M. Prost, Phys. Rev. Lett. **43**, 1654 (1979).
- <sup>8</sup>A. Bordenave-Montesquieu, A. Gleizes, and P. Benoit-Cattin, Phys. Rev. A **25**, 245 (1982).
- <sup>9</sup>Q. C. Kessel, R. Morgenstern, B. Muller, and A. Niehaus, Phys. Rev. A **20**, 804 (1979).
- <sup>10</sup>R. Morgenstern, A. Niehaus, and U. Thielmann, J. Phys. B **10**, 1039 (1977).
- <sup>11</sup>Equivalently one could introduce an initial distorted wave function:  $\Psi_j^+ = \Phi_j(\mathbf{r}_{T_1}, \mathbf{r}_{T_2}) D^-(a, -\mathbf{v}, \mathbf{r}_{P_1}) D^-(a, -\mathbf{v}, \mathbf{r}_{P_2}) \sim \Phi_j(\mathbf{r}_{T_1}, \mathbf{r}_{T_2}) (At)^{2ia}$  for  $t \gg A$ , which produces the same effect.
- <sup>12</sup>I. M. Chesire, J. Phys. B (Proc. Phys. Soc.) **10**, 428 (1968), Eq. 37.
- <sup>13</sup>I. S. Gradshteyn and I. Ryzhik, *Tables of Integrals, Series and Products* (Academic, London, 1977), p. 1060.
- <sup>14</sup>Y. L. Luke, *Mathematics in Science and Engineering* (Academic, New York, 1969), p. 226.
- <sup>15</sup>Y. L. Luke, Ref. 14, p. 170.
- <sup>16</sup>The limits of the Meijer's functions are
- $$G_{2\ 3}^{3\ 1}(z | \begin{smallmatrix} -n, 1 \\ -n+2, -n+1, -n \end{smallmatrix}) \rightarrow \begin{cases} z^{-n}/n! & \text{as } z \rightarrow 0 \\ 2z^{-n-1}/(n+1)! & \text{as } z \rightarrow \infty \end{cases} .$$
- The first order  $G_{1\ 2}^{2\ 1}(z | \begin{smallmatrix} - \\ 0, -1 \end{smallmatrix})$  can be also written as  $G_{2\ 3}^{3\ 1}(z | \begin{smallmatrix} -1, 1 \\ 1, 0, -1 \end{smallmatrix})$ , and the limits above apply.
- <sup>17</sup>According to the experiments, the  $^1D$  state accounts for most of the yield. For example, at 2 keV He<sup>+</sup>-He collision,  $^1D_0$  represents 11% of the total, while  $^1P_0$  only for 0.6 percent (see Ref. 9), and sometimes neglected (as in Ref. 8).
- <sup>18</sup>I. S. Gradshteyn and I. Ryzhik, Ref. 13, p. 497.
- <sup>19</sup>*Handbook of Mathematical Functions*, Natl. Bur. Stand. Appl. Math. Ser. No. 55, edited by M. Abramowitz and I. Stegun (U.S. GPO, Washington, D.C., 1965), Chap. 13.
- <sup>20</sup>I. S. Gradshteyn and I. Ryzhik, Ref. 13, p. 860.
- <sup>21</sup>If we write the first and second orders as  $G_{3\ 3}^{3\ 1}$  (see Ref. 12), then their Laplace transformations can also be written as Meijer's functions  $G_{3\ 3}^{3\ 2}$  (see Ref. 14, p. 166).
- <sup>22</sup>In some way, this uncertainty is also present in Ref. 7, where a phase was unknown, namely  $\beta_{n,m}$  in that article, which was there set to be zero for simplicity.